Oldeman, BE., Champneys, AR., & Krauskopf, B. (2003). Homoclinic branch switching: A numerical implementation of Lin's method. *International Journal of Bifurcation and Chaos*, *13*(10), 2977-2999. https://doi.org/10.1142/S0218127403008326

Homoclinic branch switching: a numerical implementation of Lin's method

Bart E. Oldeman, Alan R. Champneys and Bernd Krauskopf

Applied Nonlinear Mathematics Research Report 2001.11

August 30, 2001

Abstract

We present a numerical method for branch switching between homoclinic orbits to equilibria of ODEs computed via numerical continuation. Starting from a 1-homoclinic orbit our method allows us to find and follow an N-homoclinic orbit, for any $N > 1$ (if it exists nearby). This scheme is based on Lin's method and it is robust and reliable.

The method is implemented in AUTO/HomCont. A system of ordinary differential equations introduced by Sandstede featuring inclination and orbit flip bifurcations and homoclinic-doubling cascades, is used as a test bed for the algorithm. It is also successfully applied to reliably find multi-hump travelling wave solutions in the FitzHugh-Nagumo nerve-axon equations and in a 4th-order Hamiltonian system arising as a model for water waves.

1 Introduction

Homoclinic orbits are the key to understanding the dynamics of many systems; see for instance (Gaspard et. al. 1993) and the examples in Section 4. Once a first numerical approximation to a homoclinic is known, it can then be followed with the software HomCont (Champneys and Kuznetsov 1994, Champneys et. al. 1996), which is part of the package AUTO (Doedel et. al. 1997, Doedel et. al. 2001). Often there are many other homoclinic orbits near a given homoclinic orbit and it is, therefore, highly desirable to 'switch' from one homoclinic orbit to another and then follow the new homoclinic orbit. The key problem here is to find a good approximation of the new homoclinic orbit from information on the old homoclinic orbit.

In this paper we present a numerical method for branch switching that allows one to switch from a 1-homoclinic orbit to a nearby N-homoclinic orbit if it exists there. Here, an N-homoclinic orbit is one that passes near the equilibrium $(n-1)$ times before closing up. Previous methods for computing N-homoclinic orbits have typically either used a shooting strategy (see for instance (Champneys and Spence 1993)) or have switched indirectly using intermediate periodic orbits (Kuznetsov et. al. 2000, Oldeman et. al. 2000). An exception to this is the work of (Sandstede et. al. 1997) where, close to an orbit flip bifurcation in a reversible system, N-homoclinic orbits are constructed directly. Our approach is along similar lines to this latter work, but does not require any a priori knowledge or the computation of any additional periodic orbits.

The theoretical basis of our technique is Lin's method (Lin 1990, Sandstede 1993, Yew 1999), also known as the HLS (Hale-Lin-Sandstede or Homoclinic Lyapunov-Schmidt) method. It is an analytic technique for defining bifurcation equations close to heteroclinic connections in systems of ODEs. Lin's method uses the concept of the adjoint to the heteroclinic orbit at well-defined Poincaré sections in order to construct generalized nearby orbits with gaps in a lower dimensional space. Zeros of appropriately defined algebraic equations in this reduced space correspond to solutions close to the unperturbed heteroclinic orbit. In that way it is akin to Lyapunov-Schmidt reduction.

Our method switches from a 1-homoclinic to an N-homoclinic orbit by successively opening and then closing a sequence of Lin-gaps. It is fully implemented in the HomCont toolbox of AUTO and it will be included in a release of AUTO2000. Out method appears to be very robust and can be used to find any homoclinic orbit required, including cases with multiple N-homoclinic orbits. This is demonstrated close to certain codimension-two homoclinic bifurcations, called orbit flip and inclination flip bifurcations, which are known to result in the existence of either a single 2-homoclinic orbit or a fan of N-homoclinic orbits depending on certain open conditions (Sandstede 1993, Kisaka et. al. 1993*a*, Kisaka et. al. 1993*b*, Naudot 1996, Homburg et. al. 1994). We also apply our method to Shil'nikov-type N-homoclinic orbits to a saddle-focus (Shil'nikov 1969, Belyakov and Shil'nikov 1990), and (at a lower codimension) to the important class of Hamiltonian or reversible systems (Champneys and Groves 1997, Sandstede et. al. 1997, Champneys 1998, Champneys 1999, Peletier and Troy 2001).

The organisation of this paper is as follows. In Section 2 we describe Lin's method in detail and explain how we use it in our algorithm. Section 3 describes the implementation in AUTO/HomCont and illustrates it with computations near inclination flip and orbit flip bifurcations in Sandstede's model. In Section 4 we show how the method works for two applications,

namely travelling wave ODEs of the FitzHugh-Nagumo equations and a 5th order Korteweg-De Vries model. We draw conclusions and point to future research in Section 5.

2 Homoclinic branch switching

In this section we begin with a brief presentation of Lin's method applied to homoclinic orbits. It is used to set up a boundary-value problem for a truncated homoclinic orbit, which is suitable for use in a numerical implementation. We then describe our new algorithm to switch from a 1-homoclinic orbit to an N-homoclinic orbit within such a framework.

2.1 Lin's method

Our treatment closely follows that in Yew (1999), except that we restrict attention to homoclinic orbits rather than starting from a more general chain of heteroclinic orbits. Thus the notation here is somewhat simpler.

Suppose that we have an ODE system

$$\dot{x} = f(x, \nu), \text{ where } (x, \nu) \in \mathbb{R}^n \times V \quad (0 \in V \subset \mathbb{R}^p) \tag{1}$$

and that f is a sufficiently smooth function. We assume that p is a hyperbolic equilibrium for all $\nu \in V$, and that, at $\nu = 0$, the system (1) admits a non-degenerate homoclinic orbit $h(t)$ connecting p to itself. This means that $\lim_{t\to\pm\infty} h(t) = p$ and that $T_{h(0)}W^u(p) \cap T_{h(0)}W^s(p) = \text{span}\{\dot{h}(0)\}$. The orbit $h(\cdot)$ is referred to as the primary homoclinic orbit. Without loss of generality, we may suppose that $H = h(0)$ is a point in the orbit $h(t)$ with maximal Euclidean distance from p. If necessary, perform a time-shift along the homoclinic orbit.

Let Σ be a codimension-one section perpendicular to the orbit $h(t)$ at H. Define

$$Z = [T_H W^u(p) \cap T_H W^s(p)]^{\perp} = \text{span}\{\Psi\},$$

where, due to non-degeneracy of h, Z is one-dimensional and we choose Ψ to be a normalised vector of length 1. Note that by construction $\Psi \in \Sigma$. The vector Ψ has a natural definition in terms of the adjoint variational equation

$$\dot{w}(t) = -[D_x f(h(t), 0)]^* w(t), \tag{2}$$

which has a unique (up to constant multiples) bounded solution $\psi(t)$, satisfying $\psi(0) = \Psi$. Moreover, $\psi(t) \perp (T_{h(t)}W^u(p) \cup T_{h(t)}W^s(p))$ for all t.

When $\nu \neq 0$ and small, in general we would not expect the homoclinic orbit to persist, since it is of codimension-one. However, there exist unique functions $\{q^{\pm}(t,\nu)\}$ satisfying

$$\begin{cases} q^+(\cdot,\nu):[0,\infty)\to\mathbb{R}^n \quad ; \quad q^-(\cdot,\nu):(-\infty,0]\to\mathbb{R}^n \\ \dot{q}^{\pm} = f(q^{\pm},\nu) \\ q^+(t,\nu)\in W^s(p) \quad ; \quad q^-(t,\nu)\in W^u(p) \\ q^{\pm} \text{ are smooth with respect to } \nu \\ q^{\pm}(\cdot,0) = h(\cdot) \\ q^{\pm}(0,\nu)\in\Sigma, \text{ that is, } \langle q_j^{\pm}(0,\nu)-H,\dot{H}\rangle = 0 \quad (\dot{H}=\dot{h}(0)) \\ q^-(0,\nu)-q^+(0,\nu) = \varepsilon_\infty(\nu)\Psi \in Z \\ \frac{d}{d\mu}\varepsilon_\infty|_{\nu=0} = \int_{-\infty}^{\infty}\langle\psi(t), D_x f(h(t),0)\rangle dt. \end{cases}$$

In other words, for each sufficiently small ν there exist unique piecewise-smooth solutions lying in the stable and unstable manifolds of the equilibrium p, such that the discontinuity (Lin-gap) is restricted to lie in a particular direction (namely in $Z = \text{span}\{\Psi\}$) in the transverse section Σ. This is illustrated in Figure 1(a). It can also be shown that the adjoint equation $\dot{w}(t) = -[D_x f(q^{\pm}(t,\nu),\nu)]^* w(t)$, that is, the perturbed version of (2), possesses a unique bounded solution $\varphi(t,\mu)(t\in\mathbb{R})$, such that $\varphi(\cdot,0)=\psi(\cdot)$ and $\varphi(0,\nu)$ spans a one-dimensional subspace $\mathcal{Z}(\nu)$ in Σ, where $\mathcal{Z}(0)=Z$.

The main idea we use here is that, near h, we can construct an approximation of an N-homoclinic orbit with N Lin-gaps, where $N\geq 2$ is a natural number. Define $u_0^-(\cdot,\nu)=q^-(\cdot,\nu)$ and $u_N^+(\cdot,\nu)=q^+(\cdot,\nu)$. Then for any sequence $\mathbf{T}=\{T_j\}_{j=1,\ldots,N-1}$ where $|\nu|$ is sufficiently small and the T_j's are sufficiently large, there exists a unique sequence of functions $\{u_j(t,\nu)\}$ for $j\in\{1,\ldots,N-1\}$, which satisfy

$$\begin{cases} u_j(\cdot,\nu):[0,T_j)\to\mathbb{R}^n \\ \dot{u} = f(u,\nu) \\ ||u_j(\cdot,\nu)-q^{\pm}(\cdot,\nu)|| \text{ small in an appropriate function space} \\ u_j(0,\nu)\in\Sigma, \text{ that is, } \langle u_j(0,\nu)-H,\dot{H}\rangle = 0 \\ u_j(T_j,\nu)-u_j(0,\nu) = \varepsilon_j(T_j,\nu)\varphi(0,\nu)\in\mathcal{Z}(\nu) \text{ (also for } j=N). \end{cases} \tag{3}$$

This is illustrated in Figure 1(b). Moreover, the gap sizes can be expressed as

$$\varepsilon_j(\mathbf{T},\nu) = \varepsilon_j^{\infty}(\nu) + \langle\varphi(-T_{j-1},\nu), q^+(T_{j-1},\nu)\rangle - \langle\varphi(T_j,\nu), q^-(-T_j,\nu)\rangle + \mathcal{R}_j(\mathbf{T},\nu).$$

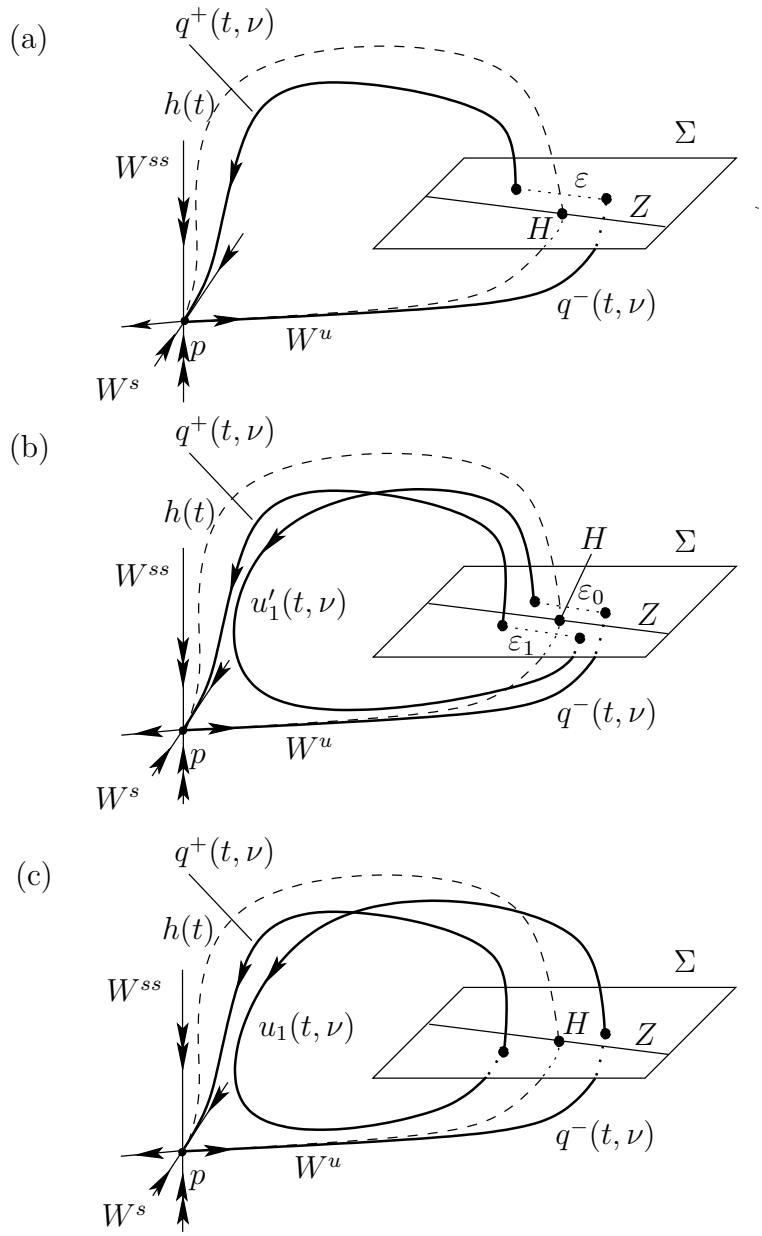

Figure 1: Lin's method applied to the homoclinic orbit. $q^{\pm}(t,\nu)$ is a perturbation of the homoclinic orbit $h(t)$ for a nearby point in parameter space ν. A dashed line is used for the trace of $h(t)$ (a). At this specific point ν in parameter space there exists a 2-homoclinic orbit, hence $q^{\pm}(t,\nu)$ can be continued to $u_1(t,\nu)$ via $u_1'(t,\nu)$ (b) and then forms a 2-homoclinic orbit together with $q^{\pm}(t,\nu)$ (c). While this is done, the gaps ε_0 and ε_1 decrease to zero.

Estimates for the remainder term $\mathcal{R}_j(\mathbf{T}, \nu)$ and its derivatives with respect to the parameter ν and the return-times T_j are given in Sandstede (1993).

A sequence of functions u_j where all Lin-gaps are closed, that is, all ε_i are zero is an N-homoclinic orbit; see Figure 1(c). In other words, the ε_i are *test functions*: they are regular smooth functions of a suitably defined boundary-value problem, whose zeros define the phenomena of interest.

In Sections 2.3 and 2.4 we show precisely how to use the parameters ν, the gap sizes ε_i and times T_i in a continuation strategy that can switch from a 1-homoclinic to an N-homoclinic orbit. First we explain how to define well-posed boundary-value problems which provide the numerical framework in which such a strategy can operate.

2.2 The truncated boundary-value problem

The method so far has been presented in an abstract analytical setting. In order to compute homoclinic orbits numerically one must somehow approximate the orbits that are defined on an infinite time interval. A natural way to do this is to truncate to some (large) finite interval and apply correct asymptotic boundary conditions (de Hoog and Weiss 1980, Lentini and Keller 1980, Beyn 1990, Friedman and Doedel 1993, Demmel et. al. 2000). The approximation of $h(t)$ is defined by truncation to a finite interval $[-T_0, T_N]$, where the right- and left-hand end points are defined by *projection boundary conditions*

$$L_s(p, \nu)(h(-T_0) - p) = 0, \quad L_u(p, \nu)(h(T_N) - p) = 0, \tag{4}$$

for suitably chosen positive values of T_0 and T_N. Here L_s and L_u are linear projection mappings onto the k-dimensional stable and $(n-k)$-dimensional unstable eigenspaces, respectively, of the equilibrium p. We can do the same to $q^{\pm}(t)$, that is, we define

$$L_s(p, \nu)(q^-(-T_0) - p) = 0, \quad L_u(p, \nu)(q^+(T_N) - p) = 0. \tag{5}$$

Due to hyperbolicity, (4) and (5) each give n boundary conditions. Physically, L_s and L_u are matrices whose columns span the appropriate eigenspaces of $D_x^T f(p)$.

We now extend the definition of $\{u_j\}$, where the individual u_j are defined either as in (3) or as follows:

$$u_0 = q^+, \qquad u_N = q^-$$

and

$$\begin{aligned} u_j[0, T_N] &= q^+[0, T_N] \\ u_j[T_N, T_N + T_0] &= q^-[-T_0, 0] \quad \text{and} \quad T_j = T_0 + T_N \end{aligned}$$

for $j = 1, \ldots, N-1$. Note that in this case, the u_j are discontinuous at $t = T_N$. Fortunately, this discontinuity is small as $T_N \to \infty$ and, hence, provided T_N is sufficiently large, these discontinuous trajectories will be good starting positions for the numerical continuation of continuous trajectories.

Now we have all the ingredients necessary to write down a boundary-value problem (BVP) for a numerical implementation of Lin's method, which is an analytical rigorous theory. They are summarized as follows:

$$\begin{cases} f(p, \nu) & = 0, & & \text{(6a)} \\ \dot{u_j}(t) - f(u_j(t), \nu) & = 0, & j = 0, \ldots, N, & \text{(6b)} \\ L_s(p, \nu)(u_0(-T_0) - p) & = 0, & & \text{(6c)} \\ L_u(p, \nu)(u_N(T_N) - p) & = 0, & & \text{(6d)} \\ \langle u_j(0) - H, \dot{H} \rangle & = 0, & j = 1, \ldots, N, & \text{(6e)} \\ u_{j-1}(T_j) - u_j(0) - \varepsilon_j \varphi(0, \nu) & = 0, & j = 1, \ldots, N. & \text{(6f)} \end{cases}$$

If the equilibrium p is fixed, then the ODE (6b) is $(N+1)n$-dimensional, and we have $k + (n-k) + N + Nn = N + (N+1)n$ boundary conditions from (6c)–(6f). This means that we need $(N + (N+1)n) - ((N+1)n) + 1 = N + 1$ free parameters to define a well-posed continuation problem. If p is not fixed, equation (6a) defines n extra problem dimensions, for which we can compensate by also continuing in the n coordinates of p.

For the specific algorithmic strategy for performing branch switching based on parameter continuation of solutions to (6a)–(6f) we now distinguish between the cases $N = 2$ and $N > 2$.

2.3 One-to-two homoclinic branch switching

In this section we describe **Algorithm 1** which can be used to switch from a 1-homoclinic to a 2-homoclinic orbit. It is illustrated in Figure 2. First we concatenate 2 approximations of the primary 1-homoclinic orbit, thereby creating the 3 pieces u_0, u_1 and u_2; see Figure 2(a).

Then we use a numerical continuation strategy to compute each u_j as a solution of a 2-point boundary-value problem. Here $N = 2$ and, hence, we have two boundary conditions involving the Poincaré section Σ (6e) and $2n$ boundary conditions for the two Lin-gaps (6f). Adding the n projection

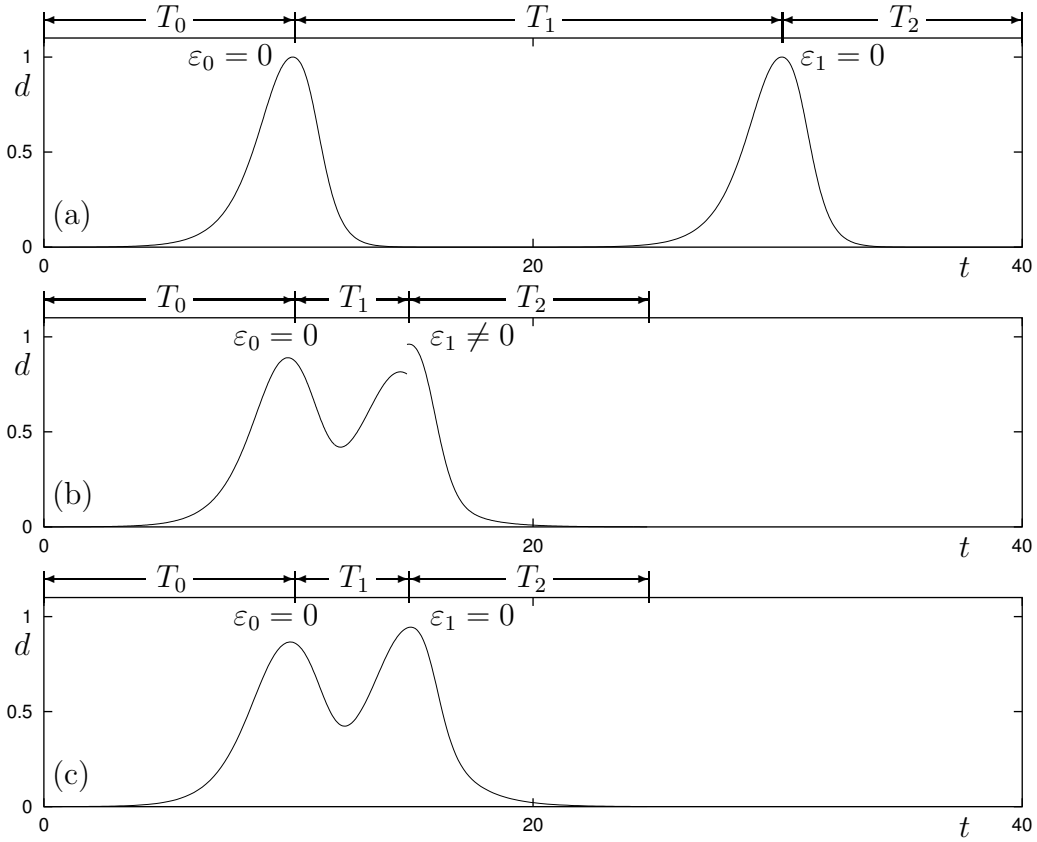

Figure 2: 1→2 homoclinic branch switching: Two copies of a 1-homoclinic orbit with the time T_1 and the gap $\varepsilon_1 = 0$ (a) are continued in $\nu_2, T_1, \varepsilon_1$, so that T_1 decreases and $\varepsilon_1 \neq 0$ (b). Continuing now in ν_1, ν_2 and ε_1 closes the gap, that is, leads to $\varepsilon_1 = 0$, which corresponds to a 2-homoclinic orbit (c). Data in this figure is obtained using Sandstede's model described in Section 3; here $d = \sqrt{x^2 + y^2 + z^2}$.

boundary conditions (6c) and (6d) for the stable and unstable manifolds near the saddle point gives a total of $3n + 2$. The phase space is $3n$-dimensional, hence we need 3 free parameters to define a regular continuation problem.

The first step (a) is to continue in the parameter ν_2, the gap ϵ_1 and the time T_1, while decreasing T_1, until ϵ_1 is large enough or T_1 is small enough. This is subject to user-defined tolerances ε_t and T_t, say, which one uses to avoid converging back to the two copies of the 1-homoclinic orbit. For illustrative purposes the case depicted in Figure 2(b) has ε_1 larger than strictly necessary.

Note that we only open one gap, that is, the gap corresponding to ε_1, and

never open the gap ε_0, as this is sufficient to find a 2-homoclinic orbit. We can now close the gap ε_1 while fixing the time T_1. This ensures that our final continuation step (b) in ν_1, ν_2 and ε_1 reaches the 2-homoclinic orbit rather than two copies of the 1-homoclinic orbit when $\varepsilon_1 = 0$; see Figure 2(c). Since all gap sizes are zero at such a point, the concatenation of u_0, u_1 and u_2 is a well-defined 2-homoclinic orbit.

The technique for 1→2 homoclinic branch switching is written in pseudo-code as **Algorithm 1**. Here *concatenate_and_split*$(h, t, 2)$ denotes the transformation of h into a data structure containing 2 copies of h. Similarly, *concatenate*$((u, T))$ combines them back into an 2-homoclinic orbit, which is only possible when all gap sizes are zero.

Algorithm 1 (1→2 homoclinic branch switching)

Input: A numerical homoclinic orbit (h, t) at $\nu = (\nu_1, \nu_2) = 0$ and threshold values T_t and ε_t. The parameter ν_2 breaks the homoclinic orbit.
Output: A numerical 2-homoclinic orbit (h', t') at $\nu' = (\nu_1', \nu_2')$.

$(u, T) = \{u_0, u_1, u_2\}, \{T_0, T_1, T_2\} \leftarrow$ concatenate_and_split$(h, t, 2)$
$\varepsilon_1 \equiv u_2(0) - u_1(1)$
repeat {step (a)}
  continue(u, T_1, ν_2, ε_1; T_1 decreasing)
until $\varepsilon_1 > \varepsilon_t$ and $T_1 < T_t$
repeat {step (b)}
  continue(u, ε_1, ν_1, ν_2; $|\varepsilon_1|$ decreasing)
until $\varepsilon_1 = 0$
$(h', t') \leftarrow$concatenate$((u, T))$

A detailed description of the implementation of the algorithm that was used to compute Figure 2 follows in Section 3.3. This particular example illustrates branch switching near an orbit flip in Sandstede's model as introduced in Section 3.2.

2.4 General one-to-N homoclinic branch switching

In this section we describe the more general **Algorithm 2** for switching from a 1-homoclinic to an N-homoclinic orbit. We illustrate this for $N = 3$ in Figure 3. Extending the situation for $N = 2$, we concatenate N approximations of the 1-homoclinic orbit, now creating the $N + 1$ pieces $u_0, \ldots, u_N$; see Figure 3(a). As explained in Section 2.2 we now need $N + 1$ free parameters to define a regular continuation problem in the $n(N + 1)$-dimensional phase space.

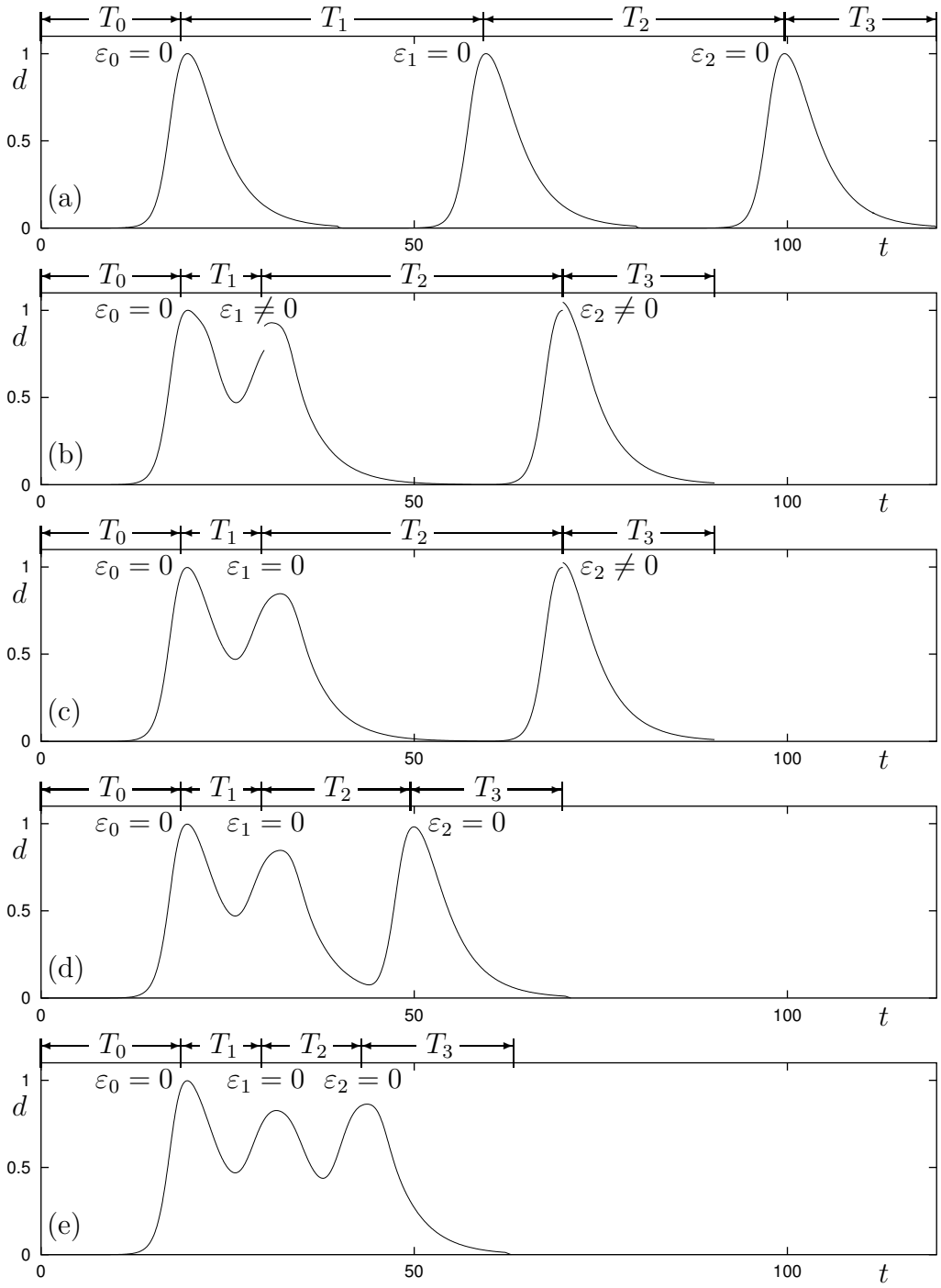

Figure 3: 1→3 homoclinic branch switching obtained similarly to Figure 2: Three copies of a 1-homoclinic orbit with the time T_1 and the gap $\varepsilon_1 = 0$ (a) are continued in $\nu_2, T_1, \varepsilon_1, \varepsilon_2$, so that T_1 decreases and $\varepsilon_1, \varepsilon_2 \neq 0$ (b). Continuing now in ν_1, ν_2, ε_1 and ε_2 closes the gap ε_1, which corresponds to a 2-homoclinic orbit (c) followed by a broken 1-homoclinic orbit. The last step closes ε_2, while continuing in ν_1, ν_2, T_2 and ε_2 to obtain two different 3-homoclinic orbits (d) and (e).

In the first step (a) these parameters are ν_2, T_1 and ε_j for $1 \leq j \leq N-1$, that is, all parameters from the $N = 2$ case plus $N-2$ extra gaps. Thus, continuing until ε_1 is large enough gives a situation like in Figure 3(b), where all Lin-gaps are open except for $\varepsilon_0 = 0$. (It can again be kept closed during branch switching). Note that, while we included extra gaps, we have not included extra times $T_j, j > 1$ among the free parameters. Continuing in more than one 'large time', that is, times of the order $T_0 + T_N$, would give convergence problems, essentially because the linearized problem is highly insensitive to each large T_j, compared with the ε_j's. (The sensitivity of the null space with respect to each large time is exponentially small while it is of order O(1) with respect to each gap ε_j.) Hence, there are step selection problems if more than one large T_j is included as a free parameter.

Algorithm 2 (1→N homoclinic branch switching)

Input: A numerical homoclinic orbit (h, t) at $\nu = (\nu_1, \nu_2) = 0$ and threshold values ε_t and T_t. The parameter ν_2 breaks the homoclinic orbit.
Output: A numerical N-homoclinic orbit (h', t') at $\nu = (\nu_1, \nu_2)$.

```
(u, T) = {u_0, ..., u_N}, {T_0, ..., T_N} ← concatenate_and_split((h, t), N)
ε_i ≡ u_i(0) − u_{i−1}(1), i = 1, ..., N
repeat {step (a)}
  continue(u, T_1, ν_2, ε_{1...N−1}, T_1 decreasing)
until ε_{1...N−1} > ε_t and T_1 < T_t
repeat {step (b)}
  continue(u, ε_{1...N−1}, |ε_i| decreasing)
until ε_{1...N−1} > ε_t and T_1 < T_t
for i = 2 to N − 1 do {step (c)}
  repeat {step (c.i)}
    continue(u, ε_{i...N−1}, T_{2...i}, ν_1, ν_2, T_i decreasing)
    if ε_i = 0 then
      report solution
    end if
  until T_i does not decrease anymore.
end for
(h', t') ←concatenate(u, T)
```

In subsequent steps (b) and (c.i) we close the gaps one-by-one. First we close the first gap ε_1, by continuing in ν_1, ν_2 and ε_j for $1 \leq j \leq N-1$. The result, such as in figure 3(c), is a concatenation of a 2-homoclinic orbit and broken 1-homoclinic orbits. In further steps (c.i), where $i \geq 2$ we fix all $\varepsilon_j, j < i$ corresponding to closed gaps and continue in ν_1, ν_2, the remaining open $\varepsilon_j, i \leq j \leq N-1$ and $T_j, 2 \leq j \leq i$. In these steps, only the last time T_i

is continued from a very large value. Each step closes ε_i and, therefore, we have effectively found an $(i+1)$-homoclinic orbit after steps (c). In certain cases there may be more than one $(i+1)$-homoclinic orbit. This is reflected by the existence of multiple zeros for ε_i as is illustrated in panels (d) and (e) of Figure 3; see also Section 3.3.4. The fact that T_2 is fixed defines an approximately fixed curve in (ν_1, ν_2)-parameter space upon which we are travelling in step (b) and all steps (c.i).

In pseudo-code the scheme for 1→N switching is in **Algorithm 2**. Note that while this scheme has the advantage of actually finding additional homoclinic orbits in intermediate steps, it is not the only possible way of closing the gaps. In principle it is possible to close the gaps in any order using continuation in the appropriate times, gaps and parameters but this algorithm does so in a systematic way. Also note that the broken 1-homoclinic orbits we obtain in steps (a) and (b) will be identical, and all gap sizes $\varepsilon_i, i > 1$ must therefore be equal after these steps. However this does not affect the end result.

In Section 3.3 we give a detailed numerical description of the implementation of the algorithm used to produce Figure 3, which illustrates branch switching near an inclination flip in Sandstede's model.

3 Implementation and illustration

After detailing the theory and algorithmic approach above, we explain here how the method works in practice. Note that our technique is based on Lin's method, which is analytically rigorous. We do not develop additional theory of the numerical method here, but demonstrate it with several examples. We give a detailed account of the implementation within the software AUTO (Doedel et. al. 1997). AUTO cannot continue discontinuous orbits natively. Hence, we have to set up a special data structure to account for the interior boundary conditions. After describing these implementation details, we shall then illustrate its use by presenting numerical results for a certain test example due to Sandstede (1997).

3.1 Implementation in AUTO

All orbits in AUTO use the time interval [0,1]. Hence we need to rescale the pieces of trajectory u_i. Define $x_i(t) = u_i(T_i t)$. Then AUTO can continue the system of pieces of trajectory u_i as an $n(N+1)$-dimensional two-point boundary-value problem. Table 1 shows the initial layout, where we concatenate N copies of the approximated 1-homoclinic orbit. Then BVP (6a)–(6f)

is transformed to the new time scale, that is, we consider:

$$\begin{cases} f(p,\nu) & = 0, \\ \dot{x_j}(t) - T_j f(x_j(t),\nu) & = 0, \quad j = 0,\ldots,N, \\ L_s(p,\nu)(x_0(0)-p) & = 0, \\ L_u(p,\nu)(x_N(1)-p) & = 0, \\ \langle x_j(0) - P, Q\rangle & = 0, \quad j = 1,\ldots,N, \\ x_{j-1}(1) - x_j(0) - \varepsilon_j R & = 0, \quad j = 1,\ldots,N, \end{cases} \tag{7}$$

where P is initialized to H, Q is initialized to $\dot{H}$ and R is initialized to Ψ.

Table 1: Initial data layout, where $-T_0$ and T_N denote the times of the numerical homoclinic solution at the left- and right-hand boundary points respectively. Note that the $n-1$ internal pieces do not represent continuous trajectories, but have small gaps between $h(T_N)$ and $h(-T_0)$. The point $H = h(0)$ is the point furthest from the equilibrium on the homoclinic orbit.

t	x_0	x_1	...	x_{N-1}	x_N
0	$h(-T_0)$	H	...	H	H
.	.	.	...	.	.
.	.	$h(T_N)$	...	$h(T_N)$	.
.	.	$h(-T_0)$	...	$h(-T_0)$	.
.	.	.	...	.	.
1	H	H	...	H	$h(T_N)$

Note that in this implementation, we assume that the Lin vector Ψ does not vary for small ν, that is, $\Psi := \varphi(0,0) = \varphi(0,\nu) = R$. This simplifies the computation a lot and is found to lead to no convergence or robustness problems in our numerical calculations.

Apart from the actual orbit, space must be allocated to the additional parameters $\{\varepsilon_j\}_{j=1,\ldots,N}$, $\{T_j\}_{j=0,\ldots,N}$, P, Q and R. At the beginning of each step, P can be initialized to $x_0(1)$, because $x_0(1) \in \Sigma$. Also, HomCont is able to find the numerical solution of the adjoint for the primary 1-homoclinic orbit $h(t)$. Hence the Lin vector $R = \Psi$ can be obtained from the computed data.

As explained in **Algorithm 1** and **Algorithm 2** above, we need to implement the procedures *concatenate_and_split* and *concatenate* to manipulate the data structures. A homoclinic orbit in HomCont is represented at a defined number `NTST` $\times$ `NCOL` of points, where `NTST` is the number of mesh intervals and `NCOL` (typically `NCOL` = 4) denotes the number of so-called

Gauss collocation points per mesh interval. The coordinates of the orbit are given as mesh points for values of the rescaled time t, where $0 \leq t \leq 1$, with the additional property that the points at $t = 0$ and $t = 1$ are close to the equilibrium along the stable and unstable linear eigenspaces, respectively.

The procedure *concatenate_and_split* transforms $h(t)$ into the initial layout given in Table 1. To do this we need to make sure that all meshes whereupon the x_i are defined are the same. Initially the three [0,1]-normalized meshes corresponding to x_0, any $x_i, i = 1, \ldots, N-1$ and x_N are all different. Hence we must merge these meshes and interpolate intermediate values. This is the key ingredient of *concatenate_and_split*. When the data structure is in the right format, we implement the boundary-value conditions given in (7) into HomCont and the actual continuation can start.

After all gaps are closed we use the procedure *concatenate* which simply appends all of the $x_{0,\ldots,N}$ and returns a normal N-homoclinic orbit that can be used for further continuation in AUTO and HomCont. This step is simpler than *concatenate_and_split* since no remeshing is required.

3.2 Test examples

We have used Sandstede's model (Sandstede 1997) as a test bed for our method. It is a theoretical model that is explicitly constructed so that it contains so-called inclination flip and orbit flip bifurcations, which involve codimension-two homoclinic orbits to a real saddle. Under certain assumptions these bifurcations generate N-homoclinic orbits for all N and, since all of the unfoldings of these bifurcations are known, they are ideal for testing whether we are able to switch between homoclinic branches near these points. The model is defined as:

$$\begin{cases} \begin{pmatrix} \dot{x} \\ \dot{y} \end{pmatrix} & = \begin{pmatrix} ax + by - ax^2 \\ bx + ay - \frac{3}{2}bx^2 - \frac{3}{2}axy \end{pmatrix} + (\tilde{\mu} - \alpha z)\nabla \mathcal{C}(x) \\ \dot{z} & = cz + \gamma xz + \alpha\beta \mathcal{C}(x) + \mu x, \end{cases} \tag{8}$$

where $\mathcal{C}(x) = x^2(1-x) - y^2 = 0$ defines a Cartesian leaf, which is an algebraic expression for the basic 1-homoclinic orbit existing in this model. For $\mu = \tilde{\mu} = 0$, together with $z = 0$ this leaf is a solution curve. If also $a = 0, b = 1$, then there is the explicit analytical solution

$$(x(t), y(t), z(t)) = (1 - \left(\frac{1-e^t}{1+e^t}\right)^2, 4e^t \frac{1-e^t}{(1+e^t)^3}, 0),$$

where a, b and c control the eigenvalues of the equilibrium 0, and they are given by

$$\lambda_{1,2} = a \pm \sqrt{b^2 + 4\tilde{\mu}^2}, \quad \lambda_3 = c.$$

We manipulate a, b and c such that one eigenvalue is positive and scaled to 1, and the other two, $-\lambda_{ss}$ and $-\lambda_s$ are negative and $-\lambda_{ss} \leq -\lambda_s < 0$. In what follows, we keep all these eigenvalues real.

For $\beta = 0$, μ and $\tilde{\mu}$ unfold an orbit flip bifurcation and for $\beta = 1$, μ and α unfold an inclination flip bifurcation. The parameter γ can be used to control normal-form coefficients in various global bifurcations present in the model, and it also serves as a non-degeneracy parameter.

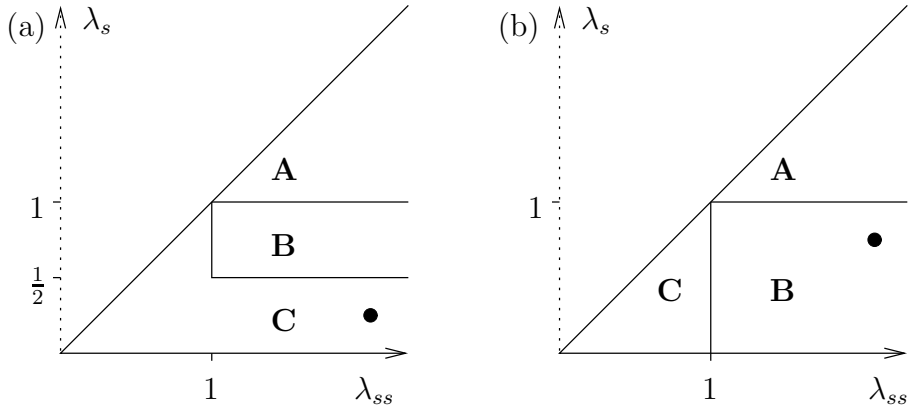

Figure 4: Eigenvalue regions corresponding to Figure 5 for different behaviour of the inclination flip (a) and the orbit flip (b). The dots denote the values (2,0.25) in panel (a) and (2,0.75) in panel (b), which correspond to the illustrations for (8) in Figures 2, 3 and 6–11.

We do not explain the geometry of inclination flip and orbit flip bifurcations, but instead refer to (Homburg et. al. 1997, Kisaka et. al. 1993*a*, Kisaka et. al. 1993*b*) for the inclination flip, and to (Sandstede 1993) for the orbit flip. The unfoldings of inclination flip and orbit flip bifurcations are summarised qualitatively in Figure 5. The cases **A** (no additional bifurcations), **B** (homoclinic doubling) and **C** (fan of many N-homoclinic orbits, n-periodic orbits for any n and chaos) depend on the eigenvalues at the equilibrium (the origin), as given in Figure 4. For an overview of the fan depicted in Figure 5 and the other possibilities for type **C** see (Homburg and Krauskopf 2000, Oldeman et. al. 2000, Oldeman et. al. 2001).

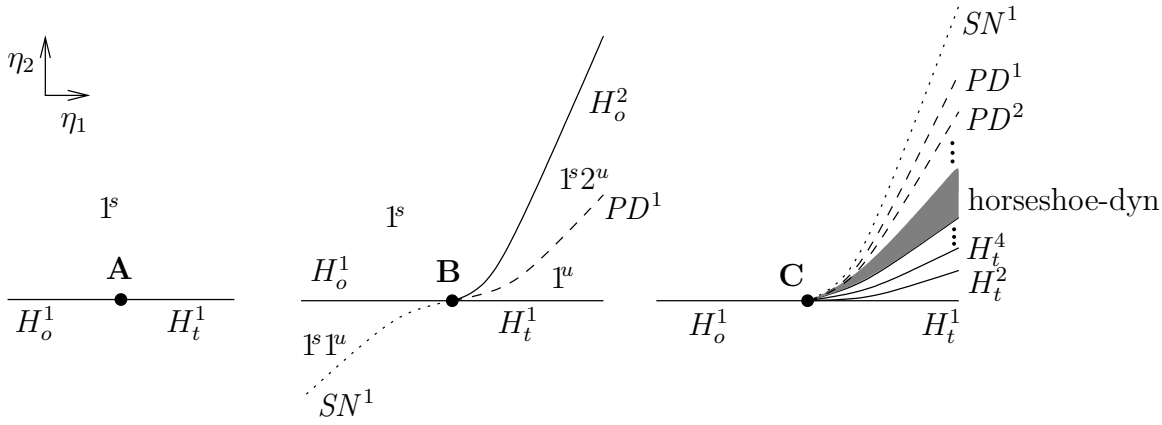

Figure 5: Codimension-two inclination flip and orbit flip bifurcation diagrams. There are three cases, **A**: no extra bifurcations, **B**: homoclinic doubling and **C**: an infinite fan of bifurcating curves and horseshoe dynamics (this is the case $\mathbf{C_{out}}$). The notation is as follows: SN^n denotes a saddle-node bifurcation of n-periodic orbits, PD^n denotes a period-doubling of an n-periodic orbit and $H^n_{t/o}$ denotes a homoclinic bifurcation of a twisted (t) or orientable (o) N-homoclinic orbit.

Specifically we consider the bifurcations occurring at the dots in Figure 4: first, the homoclinic-doubling bifurcation of type **B** occurring at an orbit flip bifurcation for $(\lambda_{ss}, \lambda_s) = (2, 0.75)$. Next, we investigate the complicated fan of bifurcations given by type **C** occurring at an inclination flip bifurcation for $(\lambda_{ss}, \lambda_s) = (2, 0.25)$.

3.3 Illustration of the method

Let us first return to Figure 2 and explain the numerical details for the computations that were applied to obtain the 2-homoclinic orbit. We consider the orbit flip homoclinic-doubling bifurcation of type **B** at $(\lambda_{ss}, \lambda_s) = (2, 0.75)$; the upper row of Table 2 gives the parameters of (8) that are used here.

Table 2: Parameter values of (8) used in the computations of Figures 2, 3 and 6–11.

Parameter	a	b	c	α	β	γ	μ	$\tilde{\mu}$
Orbit flip	-0.5	$\sqrt{2.25 - 4\tilde{\mu}^2}$	-0.75	1	0	1	free	free
Inclination flip	0.375	0.625	-0.75	free	1	3	free	0

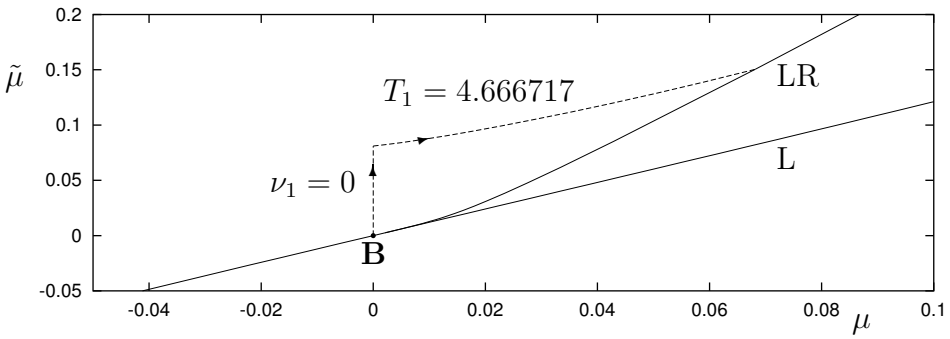

Figure 6: Parameter space diagram for 1→2 homoclinic branch switching at an orbit flip of type **B** in Sandstede's model. The explicit values are given in Table 3 and the corresponding solution graphs are in Figure 2.

Table 3: Parameter values for 1→2 homoclinic branch switching, as depicted in the panels in Figure 2 and in parameter space in Figure 6.

panel	μ	$\tilde{\mu}$	ε_1	T_1
a)	0	0	0	20
b)	0	0.0897912	-0.2	4.666717
c)	0.06814394	0.1503952	0	4.666717

An orbit flip exists for $(\mu, \tilde{\mu}) = (0, 0)$ and hence $(\mu, \tilde{\mu})$ plays the role of (ν_1, ν_2) here. Now also consider Figure 6 and Table 3. We start with 2 concatenated copies of the 1-homoclinic orbit in figure 2(a). Then, following step (a) of **Algorithm 1** we continue in $\tilde{\mu}$, ε_1 and T_1 to arrive at the orbit depicted in panel (b). For the threshold value we chose $\varepsilon_t = 0.2$ as is visible from the gap size in this panel. In practice, this threshold value can be much smaller but that would make the gaps invisible in the figures. Then, to close this gap, we follow step (b), keeping T_1 constant at 4.666717, and continue in μ, $\tilde{\mu}$ and ε_1. When $\varepsilon_1 = 0$, we have converged to the two-homoclinic orbit in panel (c). Finally, after concatenation, this two-homoclinic orbit (LR in the notation used below) was then continued in the two parameters μ and $\tilde{\mu}$, the result of which is shown in Figure 6.

Second, let us return to Figure 3 and consider switching from a 1-homoclinic to a 3-homoclinic orbit at the complicated inclination flip of type **C** at $(\lambda_{ss}, \lambda_s) = (2, 0.25)$. The parameters in (8) for this specific case are given in the lower row of Table 2. The 1-homoclinic orbit can be continued in α and μ so that an inclination flip occurs at $(\alpha, \mu) = (0.07117736, 0)$. From here on, ν_1 corresponds to $\alpha - 0.07117736$ and ν_2 corresponds to μ.

The branch switching process is also illustrated in Figure 7 and Table 4.

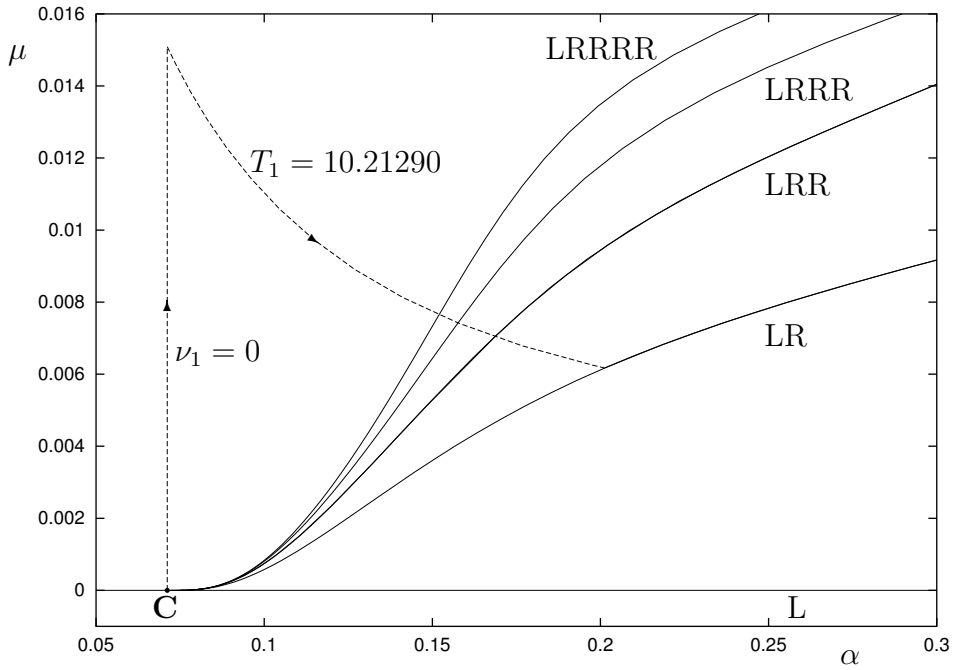

Figure 7: Parameter space diagram for 1→N homoclinic branch switching at an inclination flip of type **C**. The explicit values are given in Tables 4 and 5 and the corresponding phase space diagrams are in Figures 3, 9, 10 and 11

Table 4: Parameter values for 1→3 homoclinic branch switching, as depicted in the panels in Figure 3 and in parameter space in Figure 7.

panel	α	μ	ε_1	ε_2	T_1	T_2
a)	0.07117736	0	0	0	40	40
b)	0.07117736	15.09041×10^{-3}	0.2	0.07399750	10.21290	40
c)	0.2012851	6.172982×10^{-3}	0	0.04189286	10.21290	40
d)	0.2012857	6.172970×10^{-3}	0	0	10.21290	20.03895
e)	0.1685984	7.036245×10^{-3}	0	0	10.21290	12.00375

In this case we start with 3 concatenated copies of the 1-homoclinic orbit in figure 3(a). Following step (a) of **Algorithm 2** we continue in μ, ε_1, ε_2 and T_1 to arrive at the orbit depicted in Figure 3(b). We again chose $\varepsilon_t = 0.2$ as the threshold value. Note from this panel and Table 4 that the second gap ε_2 is smaller. Then, step (b) specifies continuing in α, μ, ε_1 and ε_2, until $\varepsilon_1 = 0$ while keeping T_1 constant at 10.21290. Panel (c) then shows that we have converged to a 2-homoclinic orbit followed by a broken 1-homoclinic orbit. The last step (c.2) involves continuation in α, μ, T_2 and ε_2, again keeping

$T_1 = 10.21290$, to close the second gap. As specified in the algorithm, instead of stopping at $\varepsilon_2 = 0$ we let the continuation proceed and find another zero and, hence, two different 3-homoclinic orbits, depicted in panels (d) and (e). These can be encoded as LRL and LRR, respectively, for 'Long Rapid Long' and 'Long Rapid Rapid'. We explain this notation in greater detail in the next section.

3.4 Using symbolic information

A strength of our method for homoclinic branch switching is that no extra information is necessary, apart from having a primary homoclinic orbit. However, if extra information on nearby N-homoclinic orbits is available then it can be used to find a prespecified number of secondary homoclinic orbits near the primary branch. We illustrate this now with the example of an orbit flip or inclination flip bifurcation of type **C**. In fact, the different homoclinic orbits can be distinguished by symbolic dynamics as we now briefly introduce; see (Homburg 1996, Homburg and Krauskopf 2000) for more details. The two 3-homoclinic orbits in panels (d) and (e) of Figure 3 differ in the time span between the humps and the closeness to the equilibrium between these humps. We can code 'L' for 'close to equilibrium' and 'R' for 'far from equilibrium', or 'L' for long and 'R' for rapid. Thus, the codings for these two 3-homoclinic orbits are LRL and LRR, respectively. Also note that Figure 3(c) in effect shows a two-homoclinic orbit LR followed by a broken one-homoclinic orbit with a Lin-gap. In the same way, the four-homoclinic orbits LRRR and LRRL can be obtained from a three-homoclinic orbit LRR followed by a broken one-homoclinic orbit. These symbolic sequences which characterize homoclinic orbits can be organized as the symbolic tree in Figure 8. This tree provides a guide how to find a particular N-homoclinic orbit in the continuation process.

We illustrate the tree with all types of N-homoclinic orbits for $N = 1, \ldots, 5$ in Figures 9, 10 and 11. We use the same inclination flip bifurcation as in Section 3.3 and keep T_1 constant at 10.21290, as shown in parameter space in Figure 7. The numerical values at which these orbits occur are given in Table 5. Note that some of these orbits are located extremely closely together in parameter space while still being far apart in phase space. This is testimony to the robustness of the method.

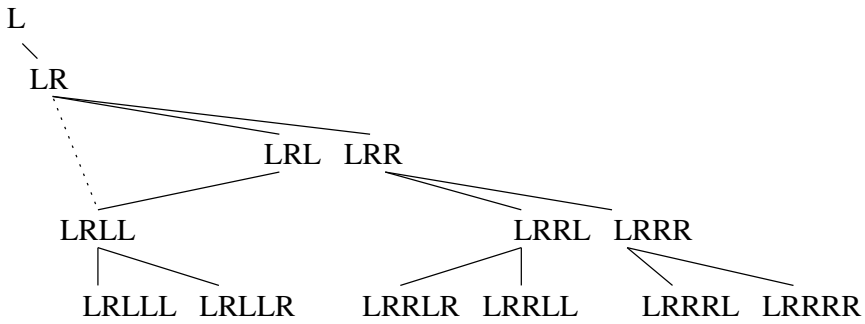

Figure 8: The symbolic tree of homoclinic orbits.

Table 5: Numerical values for the orbits in Figures 9, 10 and 11. For each of these orbits, $T_1 = 10.21290$ and the constant parameters in (8) are given in Table 2. A parameter space diagram is in figure 7.

orbit	α	μ	T_2	T_3	T_4
LR	0.2013050	6.172563×10^{-3}			
LRLL	0.2012851	6.172982×10^{-3}	20.04104	18.94592	
LRLLL	0.2012851	6.172983×10^{-3}	20.04103	18.94804	18.94592
LRLLR	0.2012851	6.172984×10^{-3}	20.03892	52.95275	10.21341
LRL	0.2012857	6.172970×10^{-3}	20.03895		
LRR	0.1685984	7.036245×10^{-3}	12.00375		
LRRLL	0.1685970	7.036292×10^{-3}	12.00371	21.98738	11.18270
LRRLR	0.1685478	7.037897×10^{-3}	12.00161	18.06557	17.26206
LRRL	0.1685472	7.037916×10^{-3}	12.00158	18.05266	
LRRR	0.1576327	7.422574×10^{-3}	11.55656	12.48667	
LRRRL	0.1575546	7.425547×10^{-3}	11.55342	12.48003	17.04167
LRRRR	0.1519881	7.646237×10^{-3}	11.32531	12.10559	12.64704

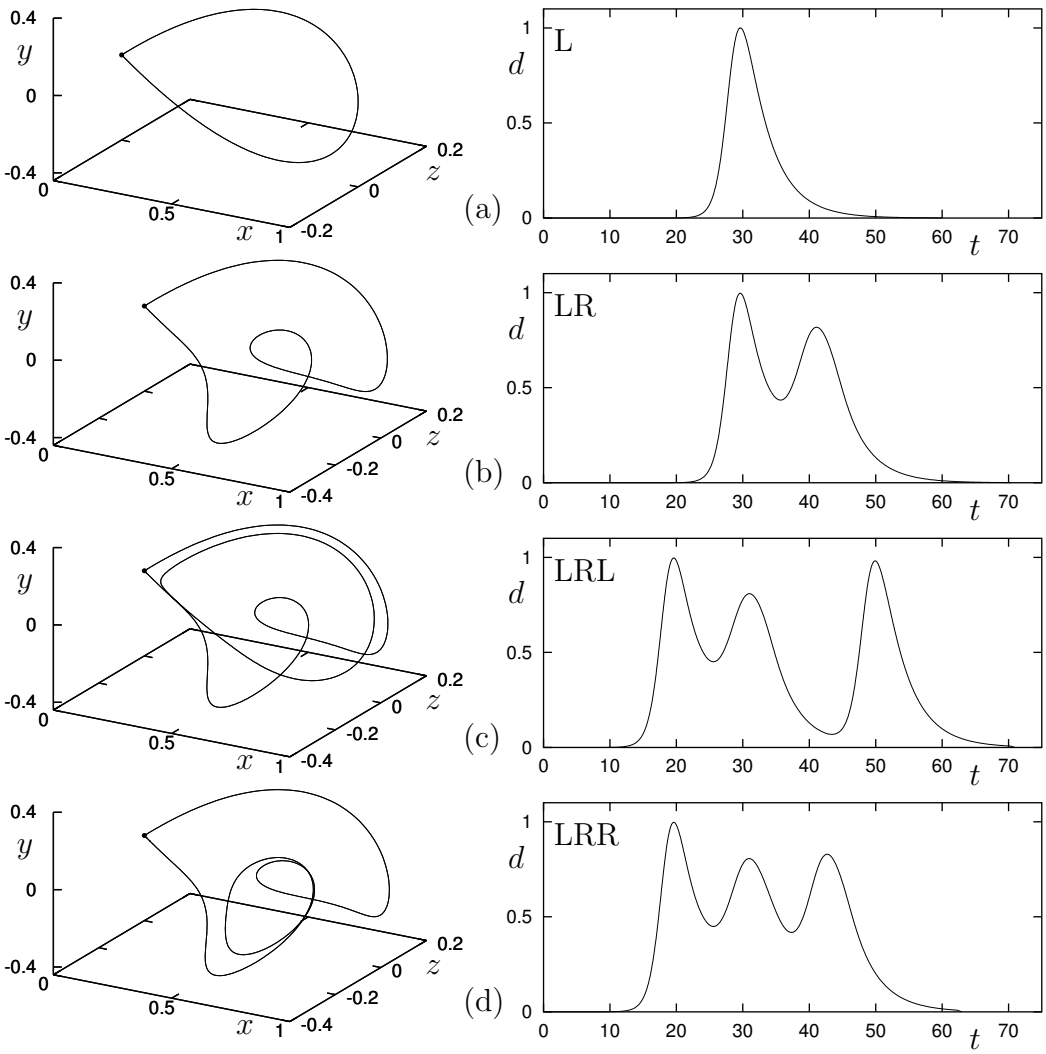

Figure 9: The 1-, 2- and 3- homoclinic orbits L (a), LR (b), LRL (c), and LRR (d). The parameter values for which these and the orbits in all subsequent figures occur are in table 5. The two 3-homoclinic orbits LRL (c) and LRR (d) were already in Figures 3(d) and (e).

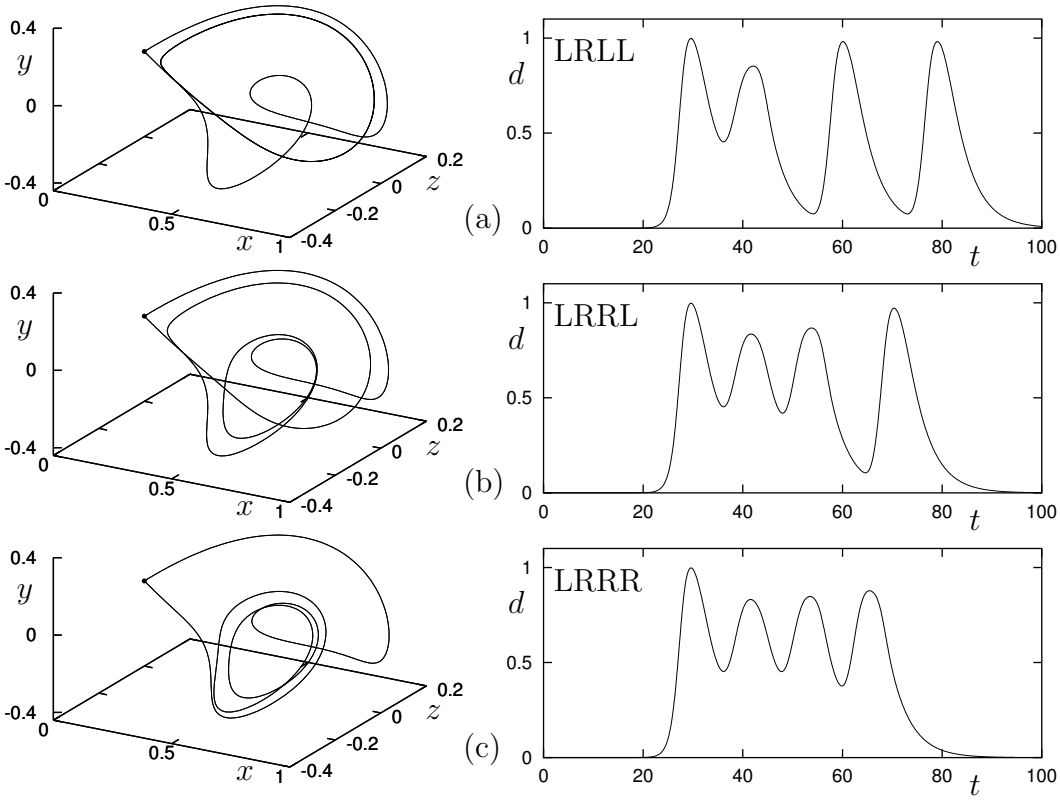

Figure 10: The 4-homoclinic orbits LRRR (a), LRRL (b), and LRLL (c).

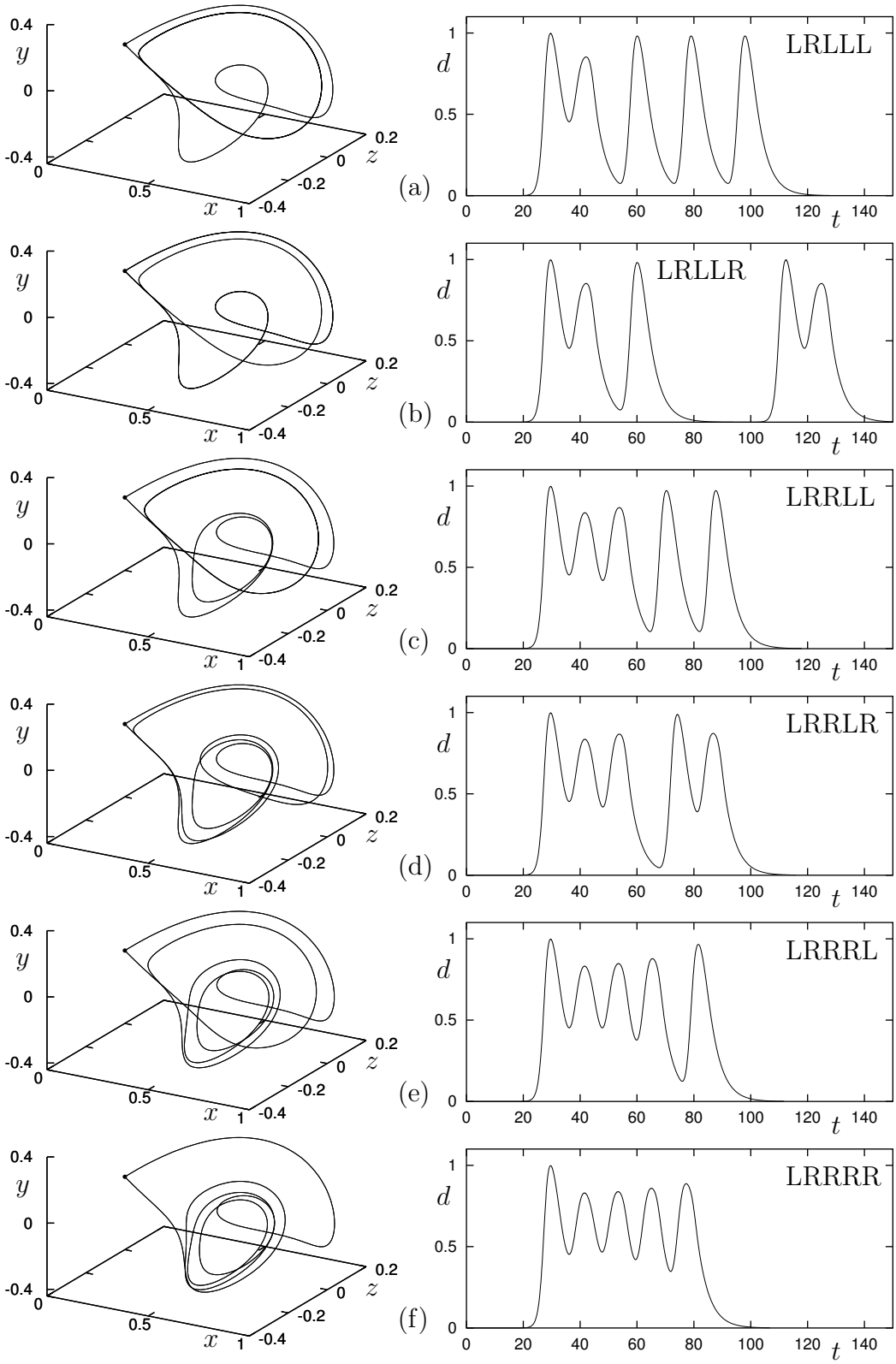

Figure 11: The 5-homoclinic orbits LRLLL (a), LRLLR (b), LRRLL (c), LRRLR (d), LRRRL (e), and LRRRR (f).

4 Applications

In this section we explore two examples which arise from applications: Shil'nikov type N-homoclinic orbits in the FitzHugh-Nagumo nerve-axon equations, and n-pulses obtained via a reversible orbit flip in a 5th order KdV model for water waves (Champneys and Groves 1997). They demonstrate that our method works for homoclinic orbits to equilibria with complex conjugate eigenvalues and in the Hamiltonian setting.

4.1 The FitzHugh-Nagumo equations

The FitzHugh-Nagumo (FHN) equations (FitzHugh 1961, Nagumo et. al. 1962) are a simplified version of the Hodgkin-Huxley equations (Hodgkin and Huxley 1952). They model nerve axon dynamics and are given by

$$\begin{aligned} u_t &= u_x x - f_a(u) - w \\ w_t &= \epsilon(u - \gamma w) \end{aligned} \tag{9}$$

where

$$f_a(u) = u(u-a)(u-1)$$

Travelling wave solutions of the form $(u,w)(x,t) = (u,w)(\xi)$, where $\xi = x + ct$ are solutions of the following ODE system:

$$\begin{aligned} \dot{u} &= v \\ \dot{v} &= cv + f_a(u) + w \\ \dot{w} &= \frac{\epsilon}{c}(u - \gamma w) \end{aligned} \tag{10}$$

In particular we consider solitary wave solutions of (9). These correspond to orbits homoclinic to $(u,v,w) = 0$ in system (10). In our numerical example we keep $\gamma = 0$. First we obtained a homoclinic orbit using a homotopy technique (see Friedman et. al. (1994)) for the parameter values $c = 0.21, a = 0.2, \epsilon = 0.0025$.

This 1-homoclinic orbit was then continued in the parameters c and a. The 1-homoclinic orbit has a Belyakov bifurcation at $(a,c) = (0.1318124, 0.2171656)$. This is a point where the saddle quality changes such that Shil'nikov chaos ensues for lower values of a; see Champneys and Kuznetsov (1994) and the references therein. For these parameter values the eigenvalues corresponding to the hyperbolic equilibrium $(u,v,w) = (0,0,0)$ are complex

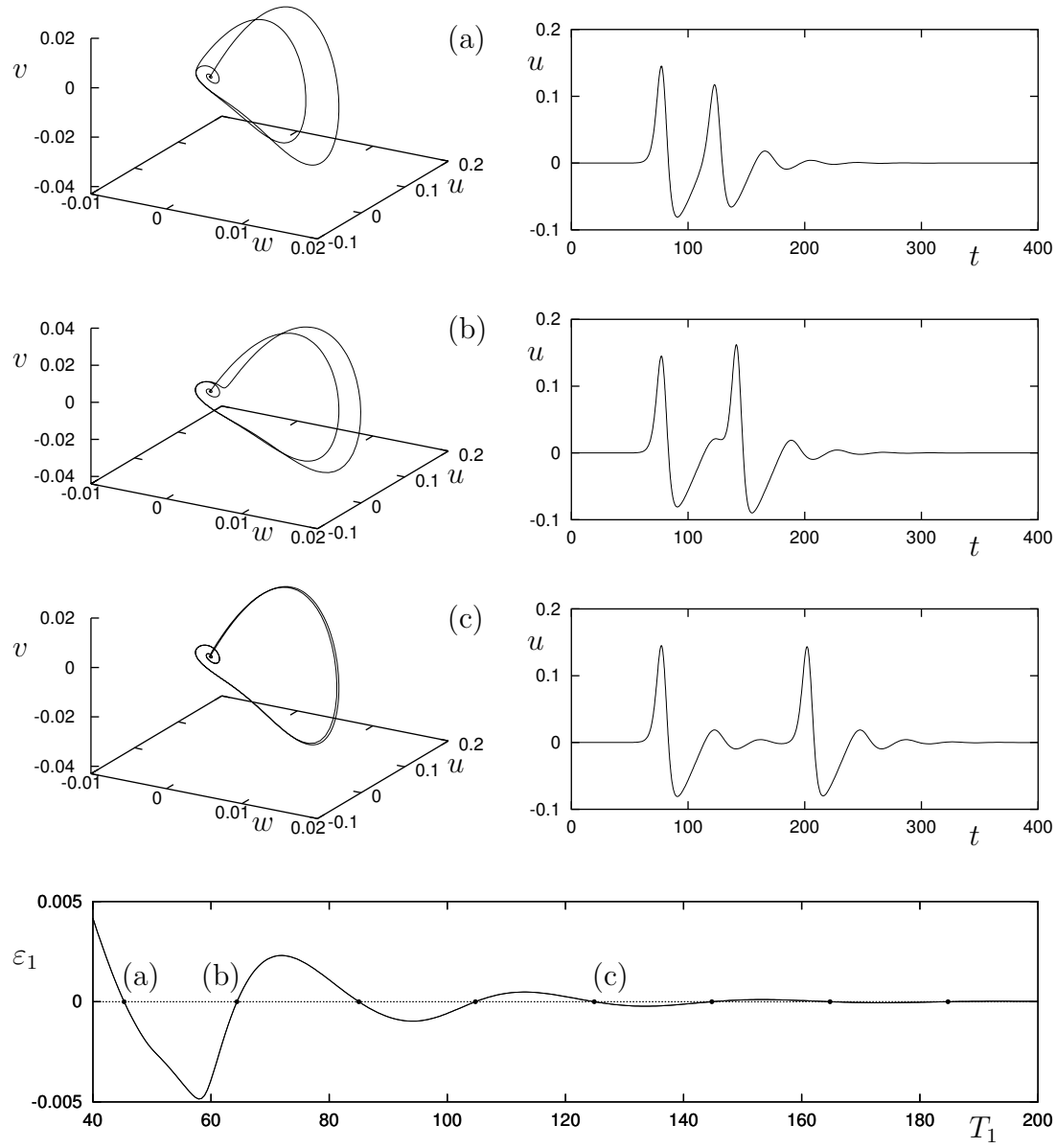

Figure 12: Bottom panel: a plot of ε_1 as a function of T_1 during our computation of Shil'nikov-type two-homoclinic orbits. Each zero corresponds to a different orbit. Also shown are the orbits for: the first zero at $T_1 = 45.28849$ (a), the second zero at $T_1 = 64.39213$ (b), and the fifth zero at $T_1 = 124.8685$ (c).

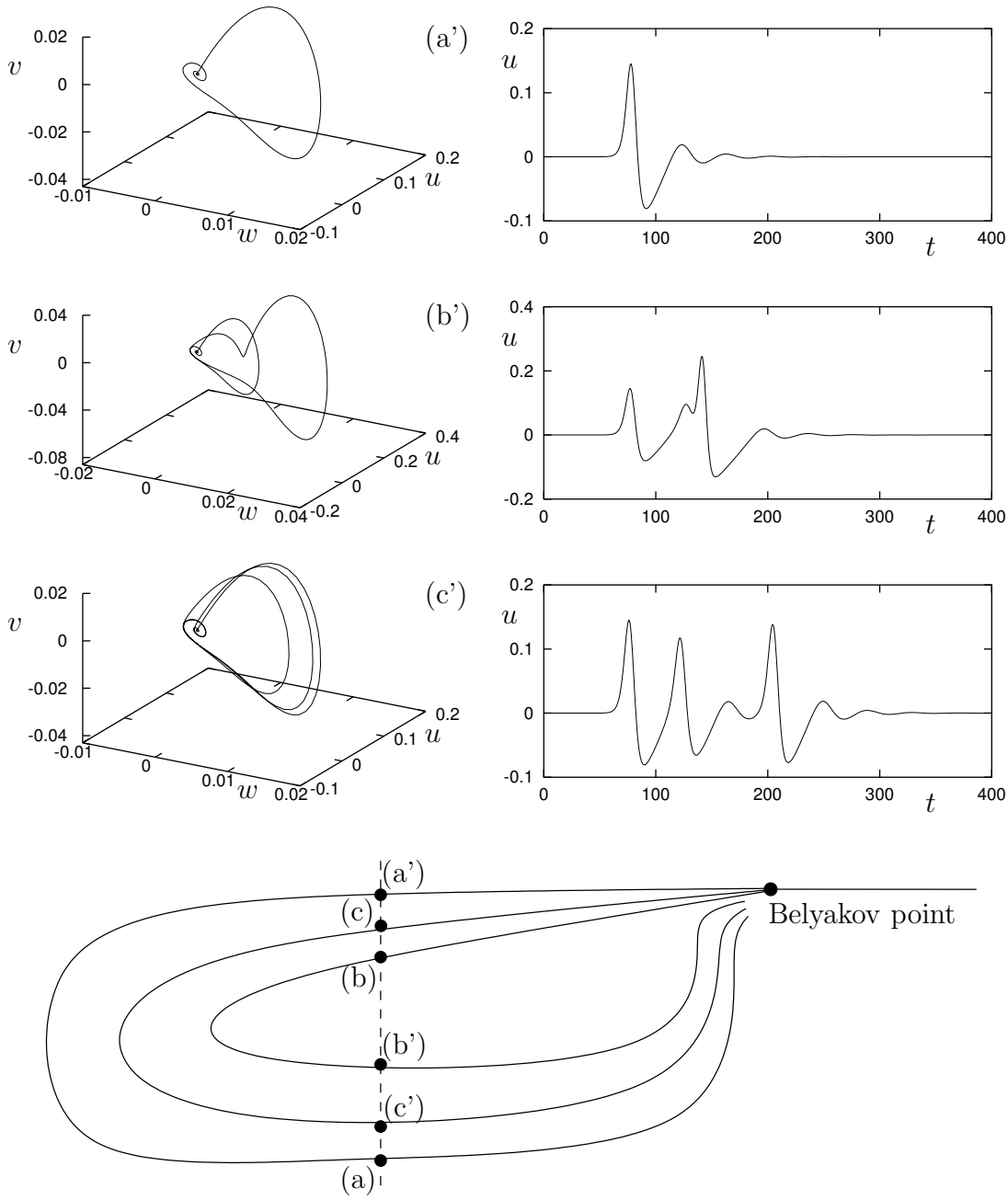

Figure 13: Bottom: conjectured bifurcation diagram of homoclinic bifurcation curves emerging from a Belyakov point for the Fitzhugh-Nagumo equations. When the orbits (a), (b) and (c) from Figure 12 are continued the respective bifurcation curves fold back in parameter space while the orbits transform into those in panels (a'), (b') and (c'), respectively.

conjugate, and we have a Shil'nikov-type homoclinic orbit. We stopped the continuation at $(a, c) = (0, 0.274218)$. Here the homoclinic orbit still corresponds to a codimension-one bifurcation and is not particularly close to the Belyakov point.

Note that the continuation strategy therefore is slightly different from **Algorithm 1** and **Algorithm 2** above, because our starting point is of codimension-one. To find higher order homoclinic orbits one can skip step (b) in these algorithms and for steps (c) in **Algorithm 2** one of the ν_i parameters has to be substituted by T_1. Also, theoretically the adjoint vector is not well defined in the limits $t \to \pm\infty$. Nevertheless, HomCont returns a vector Ψ that can be successfully used to play the role of 'Lin vector' in our computations.

Starting from this 1-homoclinic orbit we computed N-homoclinic orbits by perturbing in the direction of the parameter c, that is by continuing in the parameters ε_1, T_1 and c for decreasing T_1 until we obtain no further zeros of ε_1. We immediately obtained many different 2-homoclinic orbits, as is also predicted by the theory (Feroe 1981, Gaspard 1983, Kuznetsov 1998). The value of c was found to vary only in the 8th decimal place. The results are shown in Figure 12 by a plot of ϵ_1 versus T_1, together with the 2-homoclinic orbits corresponding to the first (a), second (b) and fifth (c) zero for increasing T_1.

It is now possible to continue in two parameters the homoclinic orbits in Figure 12 (a), (b) and (c) and this reveals an interesting structure near the Belyakov point. The curve of the primary 1-homoclinic orbit loops back reaching its minimum value of a at $(a, c) = (-0.01466826, 0.2873521)$ and returns close to the Belyakov point. In this process, the 1-homoclinic orbit is continuously transformed into a 2-homoclinic orbit; see Figure 13(a'). This 2-homoclinic orbit in Figure 12(a) is indeed one that we found with our branch-switching algorithm. The bifurcation curves of the orbits in Figure 12(b) and (c) similarly loop back reaching their minimal values of a at $(a, c) = (-0.009657518, 0.2825630)$ and $(a, c) = (-0.01466827, 0.2873523)$, respectively. On return towards the Belyakov point they are transformed into the orbits depicted in Figure 13(b') and (c').

This short example shows how homoclinic branch switching can be used to unravel complicated bifurcation structures in the FHN equations. The results of our work are summarized by the sketch of the bifurcation diagram in Figure 13. We stress that this bifurcation diagram is conjectural and difficult to depict numerically because all the bifurcation curves of N-homoclinic orbits are numerically overlaid, tracing approximately the same curve in the (a, c)-plane as the primary 1-homoclinic orbit. Because of convergence problems with AUTO our numerical results do not make clear whether the bi-

furcation curves of the homoclinic orbits head back to the Belyakov point or pass it closely, leading to new Belyakov points on these branches, as was for example found in Kuznetsov et. al. (2000). Details of this bifurcation structure remain a topic for further research.

4.2 Solitary wave solutions to a fifth-order two-parameter model equation for water waves

In (Champneys and Groves 1997) the following water wave model was considered:

$$\frac{2}{15}r^{iv} - br'' + ar + \frac{3}{2}r^2 - \frac{1}{2}(r')^2 + [rr']' = 0. \tag{11}$$

It represents solitary-wave solutions $r(x+at)$, $r \to 0$ as $x \to \pm\infty$ of the 5th order PDE

$$r_t + \frac{2}{15}r_{xxxx} - br_{xxx} + 3rr_x + 2r_x r_{xx} + rr_{xxx} = 0,$$

where a is the wave speed. The ODE corresponds to a Hamiltonian system with Hamiltonian

$$H = -\frac{1}{2}q_1^3 - \frac{1}{2}aq_1^2 + p_1q_2 - \frac{1}{2}bq_2^2 + \frac{15}{4}p_2^2 + \frac{1}{2}q_2^2q_1$$

and

$$q_1 = r, \quad q_2 = r', \quad p_1 = -\frac{2}{15}r''' + br' - rr', \quad p_2 = \frac{2}{15}r''.$$

System (11) is reversible under the transformation $t \mapsto -t, (q_1, q_2, p_1, p_2) \mapsto (q_1, -q_2, -p_1, p_2)$. It exhibits an orbit flip for a reversible system. In Hamiltonian systems, homoclinic orbits are codimension-zero phenomena, and we have to add an additional parameter λ that breaks the Hamiltonian structure in this system, by introducing artificial friction. Thus, the actual system of equations that is used for continuation is

$$\dot{x} = (\lambda I + J)\nabla H(x),$$

where $x = (q_1, q_2, p_1, p_2)$ and J is the usual skew symmetric matrix in $\mathbb{R}^4$. It is now possible to continue a homoclinic orbit in HomCont in two parameters (λ and either a or b); see also Beyn (1990).

An explicit solution exists for $a = 3/5(2b+1)(b-2), b \geq -1/2$, and it is given by

$$r(t) = 3(b + \frac{1}{2})\mathrm{sech}^2\left([\frac{3}{4}(2b+1)]^{1/2}t\right).$$

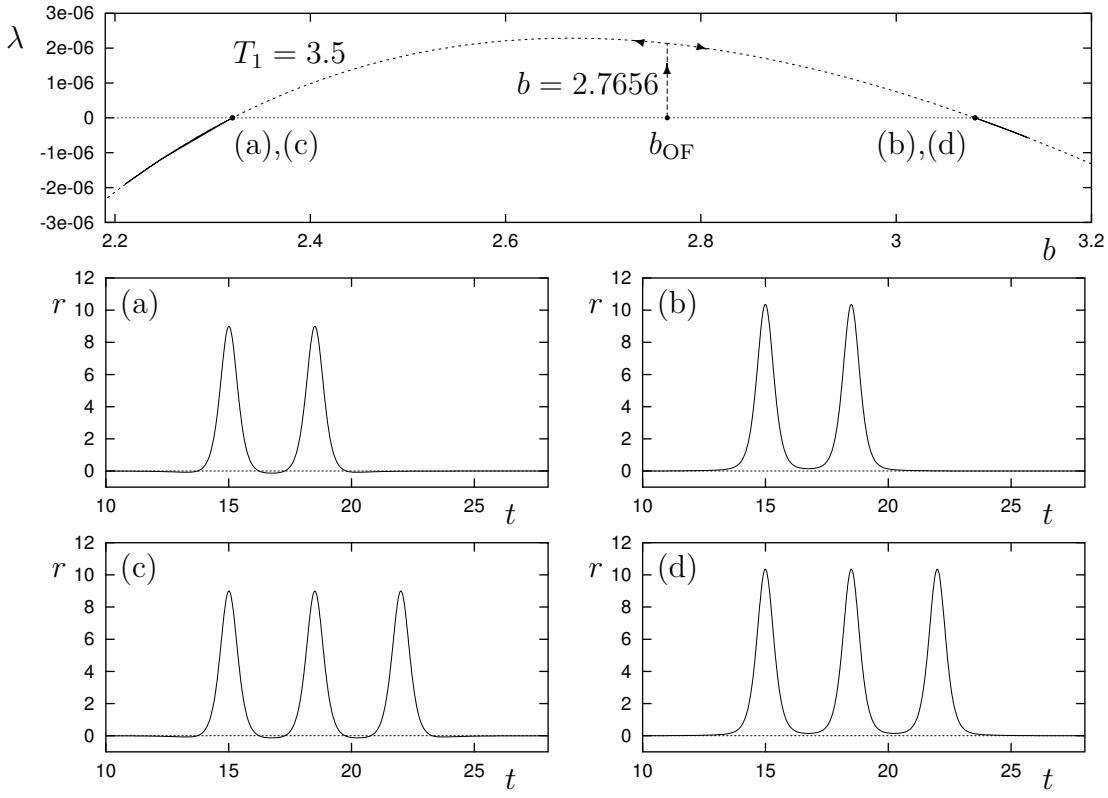

Figure 14: Branch switching in a Hamiltonian system. Starting from the reversible orbit flip bifurcation at $b = b_{\rm OF}$ we continue in λ until $T_1 = 3.5$, and then find 2-homoclinic orbits both when decreasing b (a) and when increasing b (b). Similarly one can find 3-homoclinic orbits (c) and (d), which exist at almost the same points in parameter space.

For $b > 2$ ($a > 0$) this defines an orbit flip bifurcation. We used this solution as a starting point for $a = 3, b = b_{\rm OF} = (3+\sqrt{65})/4$. Then we perturbed the orbit in $\varepsilon_i, i \geq 1$, T_1, b and λ, exactly as for the orbit flip in Section 3.2, where now $\nu = (b, \lambda)$. We know from an analysis of the orbit flip in a Hamiltonian system, that, in general there exists one N-homoclinic orbit for any N on both sides of the orbit flip bifurcation, that is, for $b > b_{\rm OF}$ and for $b < b_{\rm OF}$. Note that in contrast to the non-reversible orbit flip bifurcations all of these homoclinic orbits co-exist at any given point in an open set in the parameter space (a, b) and must necessarily be located on the line $\lambda = 0$.

The strategy of our method is depicted in Figure 14. The first step

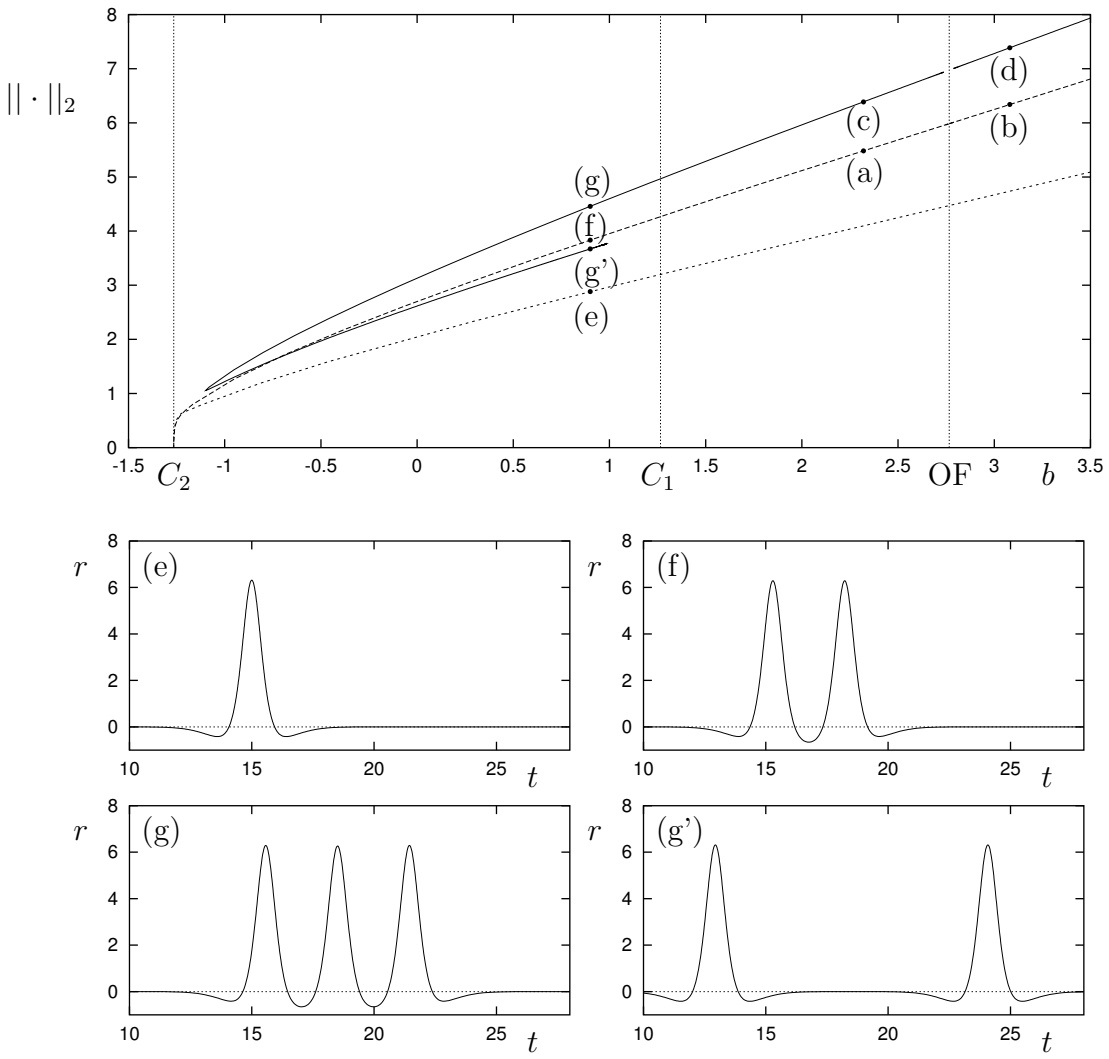

Figure 15: The AUTO L^2-norms of the orbits in Figure 14 plotted as a function of b. The 1-homoclinic (e) and 2-homoclinic (f) orbits first become of Shil'nikov-type at the Belyakov bifurcation at C_1, and then both disappear at the Hamiltonian Hopf bifurcation at C_2. The 3-homoclinic orbit (g), on the other hand, loops back and becomes a 2-homoclinic orbit (g'), approximating two copies of the 1-homoclinic orbit on its way towards the Belyakov point C_1. The labels (a), (b), (c), and (d) indicate the locations of the respective homoclinic orbits in Figure 14.

involves continuing in $\varepsilon_i, i \geq 1$, T_1 and λ. We stopped the continuation at $T_1 = 3.5$. In the next step we closed the gap corresponding to ε_1 by continuing in $\varepsilon_i, i \geq 1$, b and λ, both for increasing b and for decreasing b. In this way, we found 2-homoclinic orbits for the b-values 2.320513 and 3.080683, where $\lambda = 0$ up to numerical tolerance. These are depicted in panels (a) and (b) of Figure 14, respectively. A second gap ε_2 can be closed by continuing in $\varepsilon_i, i \geq 2$, T_2, b and λ, to find 3-homoclinic orbits at $b = 2.319957$ and $b = 3.080876$

and $\lambda = 0$ for both cases; see Figure 14(c) and (d). This continuation step involves a small loop in the (b, λ)-plane, which is approximately overlaid on the curve defined by $T_1 = 3.5$ within the solid parts depicted in Figure 14.

Once these new homoclinic orbits were found by branch switching we explored what happens to them as they are continued in b. The results are depicted in Figure 15, where we plot the L^2-norm as computed by AUTO of the 1-, 2- and 3-homoclinic orbits versus b. The positions (a), (b), (c) and (d) of Figure 14 are labelled. For increasing b nothing interesting seems to happen. For decreasing b, all three orbits first undergo a Belyakov bifurcation at $C_1(b = \sqrt{1.6} \approx 1.26491)$, just like in the FitzHugh-Nagumo system described in Section 4.1, where the eigenvalues of the equilibrium become complex conjugate. The 1- and 2-homoclinic orbits then disappear at $C_2(b = -\sqrt{1.6} \approx -1.26491)$, where the equilibrium goes through a Hamiltonian Hopf bifurcation and, hence, becomes non-hyperbolic. However, the bifurcation curve of the 3-homoclinic orbit loops back at $b = -1.099277$ and appears to go back to the Belyakov point. In this process, the middle hump lowers and the 3-homoclinic orbit is transformed into a 2-homoclinic orbit, whose humps move apart so that it approximates two copies of the 1-homoclinic orbit near the Belyakov point, much like in the example in Section 4.1.

Note that we aimed to find orbits for specific values of T_1. In many other situations it is desirable to find a certain N-homoclinic orbit at a specific value of (a, b). In those cases a strategy like in Section 4.1 should be used. Also note that in our branch switching technique we do not exploit any symmetry, although it is straightforward to reformulate the method to make this possible.

5 Conclusion

We presented a novel method for locating and obtaining an N-homoclinic orbit nearby a 1-homoclinic orbit. No additional information is required, except for a suspicion that a nearby N-homoclinic orbit may exist. Our method is fully implemented in AUTO/HomCont and can be applied in a variety of ways, as was illustrated in Section 4.

Our technique of direct branch switching is especially useful to obtain orbits which are difficult or cumbersome to get using previous indirect methods such as those applied in (Oldeman et. al. 2001). For instance, a 3-homoclinic orbit bifurcating from a saddle-type limit cycle is hard to find using those indirect techniques, while it is straightforward to find using direct algorithm switching as in Section 3.3. Furthermore, we have provided an algorithmic

way of generating many N-homoclinic orbits when they exist, such as in the example in Section 4.1, which has infinitely many Shil'nikov-type 2-pulse orbits. This can be used as a starting point of an in-depth analysis of the global structure of these 2-pulses, as was conducted for a different example in (Kuznetsov et. al. 2000) where the initial 2-pulses were obtained by a laborious method.

Moreover, with our technique one can effectively use symbolic information to find *specific* N-homoclinic orbits, given that the qualitative structure of the bifurcation is known. This was illustrated in Section 3.4 for an orbit flip bifurcation of type **C**. Interesting additional work would be to compare the numerical results we have obtained to analytical estimates by Sandstede (1993), which are valid in a small neighborhood of the codimension-two point. A final, specialized application of our method might be for specialists who want to compute all N-pulse orbits to unveil the structure of the symbolic sequences of these orbits as we touched upon in Section 3.4.

Further refinements to our method can be made by combining k-homoclinic orbits and l-homoclinic orbits into $k + l$-homoclinic orbits. This can be especially useful for N-homoclinic orbits where N is large. However, even for large N our present method, while not the most efficient, is sufficient to find all these orbits and is ready for use in applications.

Acknowledgements

We thank Björn Sandstede and Ale Jan Homburg for helpful discussions regarding Lin's method and symbolic dynamics, and Sebius Doedel and Randy Paffenroth for supporting the implementation in AUTO.

References

Belyakov L A and Shil'nikov L P 1990 Homoclinic curves and complex solitary waves *Selecta Math. Sov.* **9**, 219–221.

Beyn W J 1990 The numerical computation of connecting orbits in dynamical systems *IMA J. Numer. Anal.* **9**, 379–405.

Champneys A R 1998 Homoclinic orbits in reversible systems and their applications in mechanics, fluids and optics *Physica D* **112**, 158–186.

Champneys A R 1999 Homoclinic orbits in reversible systems ii: Multibumps and saddle-centers *CWI Quart.* **12**, 185–212.

Champneys A R and Groves M 1997 A global investigation of a solitary wave solutions to a fifth-order two-parameter model equation for water waves *Journal of Fluid Mechanics* **342**, 199–229.

Champneys A R and Kuznetsov Y A 1994 Numerical detection and continuation of codimension-two homoclinic bifurcations *Int. J. Bifurcation and Chaos* **4**(4), 785–822.

Champneys A R, Kuznetsov Y A and Sandstede B 1996 A numerical toolbox for homoclinic bifurcation analysis *Int. J. Bifurcation and Chaos* **6**(5), 867–887.

Champneys A R and Spence A 1993 Hunting for homoclinic orbits in reversible systems; a shooting technique *Advances in Computational Mathematics* **1**, 81–108.

de Hoog F R and Weiss R 1980 An approximation theory for boundary value problems on infinite intervals *Computing* **24**, 227–239.

Demmel J W, Dieci L and Friedman M J 2000 Computing connecting orbits via an improved algorithm for continuing invariant subspaces *SIAM J. Sci. Comput.* **22**, 381–94.

Doedel E J, Champneys A R, Fairgrieve T F, Kuznetsov Y A, Sandstede B and Wang X 1997 *AUTO 97: Continuation and bifurcation software for ordinary differential equations (with HomCont).* `http://indy.cs.concordia.ca/auto`.

Doedel E J, Paffenroth R C, Champneys A R, Fairgrieve T F, Kuznetsov Y A, Sandstede B and Wang X 2001 *AUTO 2000: Continuation and bifurcation software for ordinary differential equations (with HomCont).* `http://sourceforge.net/projects/auto2000/`.

Feroe J 1981 Travelling waves of infinitely many pulses in nerve equations *Math. Biosci.* **55**, 189–204.

FitzHugh R 1961 Impulses and physiological states in theoretical models of nerve membrane *Biosphys. J.* **1**, 445–446.

Friedman M, Doedel E J and Monteiro A C 1994 On locating connecting orbits *Applied Math. And Comp.* **65**(1–3), 231–239.

Friedman M J and Doedel E J 1993 Computational methods for global analysis of homoclinic and heteroclinic orbits: A case study *J. Dyn. Diff. Eqns.* **5**, 37–57.

Gaspard P 1983 Generation of a countable set of homoclinic flows through bifurcation *Phys. Lett. A* **97**, 1–4.

Gaspard P, Arnéodo A, Kapral R and Sparrow C, eds 1993 *Homoclinic chaos. Physica D 62 (Special Issue).*

Hodgkin A L and Huxley A F 1952 A quantitative description of membrane current and its applications to conduction and excitation in nerve *J. Physiol.* **117**, 500–544.

Homburg A J 1996 *Global Aspects of Homoclinic Bifurcations of Vector Fields* Vol. 121, Number 578 (second of 4 numbers) of *Memoirs of the AMS* American Mathematical Society.

Homburg A J, Kokubu H and Naudot V 1997 Homoclinic-doubling cascades. *To appear in Arch. Ration. Mech. Anal.* `http://turing.wins.uva.nl/~alejan/Postscriptfiles/cascade.ps.gz`.

Homburg A J and Krauskopf B 2000 Resonant homoclinic flip bifurcations *J. Dyn. Diff. Eqns.* **12**(4), 807–850.

Homburg A, Kokubu H and M.Krupa 1994 The cusp horseshoe and its bifurcations in the unfolding of an inclination-flip homoclinic orbit *Ergodic Theory and Dynamical Systems* **14**, 667–693.

Kisaka M, Kokubu H and Oka H 1993*a* Bifurcations to N-homoclinic orbits and N-periodic orbits in vector fields *J. Dyn. Diff. Eqns.* **5**, 305–357.

Kisaka M, Kokubu H and Oka H 1993*b* Supplement to homoclinic-doubling bifurcation in vector fields *in* R Bamon, R Labarca, J Lewowicz and J Palis, eds *Dynamical Systems* Longman pp. 92–116.

Kuznetsov Y A 1998 *Elements of Applied Bifurcation Theory* 2nd edn Springer.

Kuznetsov Y A, de Feo O and Rinaldi S 2000 Belyakov homoclinic bifurcations in a tritrophic food chain model. *To appear in SIAM J. Appl. Math*, `http://www.math.uu.nl/publications/preprints/1158.ps.gz`, Preprint nr. 1158, Department of Mathematics, Universiteit Utrecht, The Netherlands.

Lentini M and Keller H B 1980 Boundary value problems over semi-infinite intervals and their numerical solution *SIAM J. Numer. Anal.* **17**, 577–604.

Lin X B 1990 Using Melnikov's method to solve Silnikov's problems *Proc. Roy. Soc. Edinburgh* **116A**, 295–325.

Nagumo J S, Arimoto S and Yoshizawa S 1962 An active pulse transmission line simulating nerve axon *Proc. IRE* **50**, 2061–2070.

Naudot V 1996 *Bifurcations Homoclines des Champes de Vecteurs en Dimension Trois* PhD thesis (l'Université de Bourgogne, Dijon).

Oldeman B E, Krauskopf B and Champneys A R 2000 Death of period-doublings: locating the homoclinic-doubling cascade *Physica D* **146**(1–4), 100–120.

Oldeman B E, Krauskopf B and Champneys A R 2001 Numerical unfoldings of codimension-three resonant homoclinic flip bifurcations *Nonlinearity* **14**, 597–620.

Peletier L A and Troy W C 2001 *Spatial patterns: higher order models in physics and mechanics* Birkhäuser.

Sandstede B 1993 *Verzweigungstheorie homokliner Verdopplungen* PhD thesis University of Stuttgart. `http://www.math.ohio-state.edu/~sandsted/Paper/diss.ps.gz`.

Sandstede B 1997 Constructing dynamical systems having homoclinic bifurcation points of codimension two *J. Dyn. Diff. Eqns.* **9**(2), 269–288.

Sandstede B, Jones C K R T and Alexander J C 1997 Existence and stability of n-pulses on optical fibers with phase-sensitive amplifiers *Physica D* **106**, 167–206.

Shil'nikov L P 1969 On a new type of bifurcation of multidimensional dynamical systems *Sov. Math. Dokl.* **10**, 1368–1371.

Yew A C 1999 Multipulses of nonlinearly-coupled Schrödinger equations. *To appear in Journal of Diffential Equations*, `http://www.math.ohio-state.edu/~yew/preprints/yew99-1.ps.gz`.